Supplement of Earth Surf. Dynam., 13, 941–958, 2025
https://doi.org/10.5194/esurf-13-941-2025-supplement

Earth Surface Dynamics
Open Access
EGU

Supplement of

Bayesian reconstruction of sea level and hydroclimates from coastal landform inversion: application to Santa Cruz (US) and Gulf of Corinth

Gino de Gelder et al.

Correspondence to: Gino de Gelder (gino.de-gelder@univ-grenoble-alpes.fr)

Contents of this file

Introduction

This section contains Supplementary text, as well as 6 Supplementary Figures. The text includes further details on the sea-level ranges used in this study. Table S1 provides a summary of those ranges. Figure S1 is an equivalent of Figure 2a, but with the misfit calculated on a vertical axis. and Figure S2 gives figures for parameter acceptance ratios and likelihood evolution during the model runs of the main paper figures. Figure S3 presents additional synthetic tests with more freedom to the input parameters. Figure S4 presents additional tests for the Corinth inversion with more freedom given to all sea- and lake-level nodes. Figure S5 presents inversion results of the Santa Cruz terraces with alternative values for *ipstep*, σ and *corrl*, whereas S6 presents a couple of Stacked Swath Profiles for comparison with the observed morphology of the marine terrace sequence. Figure S7 presents inversion results of the Santa Cruz terraces with alternative morphostratigraphic scenarios. Figure S8 presents a map and data from the SE Corinth Rift terraces.

Text S1.

Paleo sea-level ranges

The red boxes in Fig. 1c provide estimates of the likely range of relative sea-level (RSL) variations at far-field locations. The subdivision of boxes is based on the marine isotope stages (MIS) and their sub-stages defined by Railsback et al. (2015); with the exception of MIS 11a, which we split into three sub-stages based on the shape of the sea-level curve of Spratt & Lisiecki (2016) and the proposed two RSL highstands at the Huon Peninsula for that period (de Gelder et al., 2022). Time ranges are based on the sea-level curve of Spratt & Lisiecki (2016), with the exception of MIS 1 and MIS 2, for which we used the time ranges proposed by Kahn et al. (2015) and Clark et al. (2009), respectively.

The RSL datapoints are selected from the database of Hibbert et al, (2016), complemented with data from Murray-Wallace (2002), de Gelder et al. (2022), and Marra et al. (2023). We limited these to data older than 130 ka, and with total elevation uncertainties of less than 35 m (±17.5m). Concerning the data points from the Hibbert et al. (2016) database we applied the same filters as was done in the publication of their compilation, only using U/Th data with calcite <2%, ^{232}Th concentration <2 ppb and $\delta^{234}_{initial}$ of 147 +5/-10‰. The remaining RSL datapoints are from Stirling et al. (2001) and Andersen et al. (2010), for which we used the ±1σ uncertainties in time and elevation from the database (Hibbert et al., 2016). For the age uncertainty on the Murray-Wallace (2002) RSL estimates we used the time ranges of the red boxes as age error margins, and assigned an arbitrary elevation uncertainty of ±5 m. For de Gelder et al. (2022) we used the published time and elevation standard errors, whereas for Marra et al. (2023) we used the time ranges of the red boxes as age error margins, and assigned an elevation uncertainty of ±1 m as proposed in their paper.

In terms of the elevation ranges of the red boxes, for MIS 1 we used the proposed Mid-Holocene range by Kahn et al. (2015). For MIS 2 we used the minimum from Spratt & Lisiecki (2016) and the maximum from Gowan et al. (2022). For MIS 3 we used the minima from Spratt & Lisiecki (2016) and the maximum from Pico et al. (2016). For MIS 4, 5b, 5d, 6a, 8a, 10a and 12a we used the minima and/or maxima from Spratt & Lisiecki (2016) and Batchelor et al. (2019). For MIS 5a and 5c we used the minima from from Spratt & Lisiecki (2016) and the maxima from Creveling et al. (2017). For MIS 5e we used the minimum from Dyer et al. (2021) and the maximum from Kopp et al. (2009) and Dutton et al. (2015). For MIS 6b, 6c, 6d, 6e, 7a,

7c, 7e, 9a, 9e, 11a-1 and 11a-3 we used the minima from Spratt & Lisiecki (2016) and the maxima from the RSL data points. For MIS 7b we used the minimum from Spratt & Lisiecki (2016) and the maximum from the MIS 7a box. For MIS 7d we used the same range as MIS 6e. For MIS 8b we used the minimum from Spratt & Lisiecki (2016) and the maximum from the MIS 8c box. For MIS 8c, 9c, 9d and 12b we used the minimum and maximum from Spratt & Lisiecki (2016). For MIS 9b we used the minimum from Spratt & Lisiecki (2016) and the maximum from the MIS 9a box. For MIS 10b and 10c we used the minimum from Spratt & Lisiecki (2016) and the maximum from the MIS 10a box. For MIS 11a-2 we used the minimum from Spratt & Lisiecki (2016) and the maximum from the MIS 11a-1 box. For MIS 11b we used the minimum from Spratt & Lisiecki (2016) and the maximum from the MIS 11a-3 box. For MIS 11c we used the minima from Murray-Wallace (2002) and Marra (2023) and the maximum from Dutton et al. (2015).

We summarize the ranges and justifications in Table S1 below.

Period (MIS)	Time range (ka)	Based on	Elevation range (masl)	Based on
1	4 - 8	K2015	0 to 6	K2015
2	19 - 27	C2009	-135 to -115	SL2016; G2022
3a	36 - 43	SL2016	-85 to -31	SL2016; P2016
3b	44 - 49	SL2016	-88 to -31	SL2016; P2016
3c	50 - 57	SL2016	-82 to -31	SL2016; P2016
4	58 - 74	SL2016	-110 to -50	SL2016; B2019
5a	75 - 85	SL2016	-47 to -5	SL2016; C2017
5b	86 - 94	SL2016	-75 to -25	SL2016; B2019
5c	95 - 105	SL2016	-36 to -5	SL2016; C2017
5d	106 - 117	SL2016	-85 to -20	SL2016; B2019
5e	118 - 128	SL2016	0 to 9	K2009; D2015; D2021
6a	132 - 143	SL2016	-140 to -90	SL2016; B2019
6b	144 - 155	SL2016	-110 to -32	SL2016; dG2022
6c	156 - 163	SL2016	-114 to -32	SL2016; dG2022
6d	164 - 177	SL2016	-77 to -23	SL2016; dG2022
6e	178 - 191	SL2016	-90 to -19	SL2016; dG2022
7a	192 - 201	SL2016	-30 to 5	SL2016; dG2022; M2023
7b	202 - 207	SL2016	-38 to 5	SL2016; MIS7a range
7c	208 - 219	SL2016	-31 to 11	SL2016; dG2022

Period (MIS)	Time range (ka)	Based on	Elevation range (masl)	Based on
7d	220 - 231	SL2016	-90 to -19	MIS 6e range
7e	232 - 243	SL2016	-36 to 11	MW2002; A2010; SL2016; dG2022; M2023
8a	245 - 256	SL2016	-130 to -55	SL2016; B2019
8b	257 - 265	SL2016	-95 to -40	SL2016; MIS 8c range
8c	266 - 275	SL2016	-107 to -40	SL2016
9a	276 - 286	SL2016	-57 to -1	S2001; A2010; SL2016; dG2022
9b	287 - 304	SL2016	-70 to -1	SL2016; MIS 9a range
9c	305 - 317	SL2016	-35 to 11	SL2016
9d	318 - 321	SL2016	-33 to 9	SL2016
9e	322 - 332	SL2016	-30 to 15	S2001; MW2002; A2010; SL2016; dG2022; M2023
10a	335 - 348	SL2016	-130 to -40	SL2016; B2019
10b	349 - 354	SL2016	-102 to -40	SL2016; MIS 10a range
10c	355 - 362	SL2016	-107 to -40	SL2016; MIS 10a range
11a-1	363 - 372	SL2016	-67 to -9	SL2016; dG2022
11a-2	373 - 380	SL2016	-62 to -9	SL2016; MIS 11a-1 range
11a-3	381 - 388	SL2016	-48 to 9	SL2016; dG2022; M2023
11-b	389 - 397	SL2016	-41 to 9	SL2016; MIS 11a-3 range
11-c	398 - 414	SL2016	-6 to 13	MW2002; D2015; M2023
12a	426 - 438	SL2016	-150 to -85	SL2016; B2019

Table S1. Summary of paleo sea-level ranges as described in Text S1. A2010 = Andersen et al,. 2010; B2019 = Batchelor et al., 2019; C2009 = Clark et al., 2009; C2017 = Creveling et al., 2017; D2015 = Dutton et al., 2015; dG2022 = de Gelder et al., 2022; G2022 = Gowan et al., 2002; K2009 = Kopp et al., 2009; K2015 = Kahn et al., 2015; M2023 = Marra et al., 2023; MW2002 = Murray-Wallace, 2002; P2016 = Pico et al., 2016; S2001 = Stirling et al., 2001; SL2016 = Spratt & Lisiecki 2016

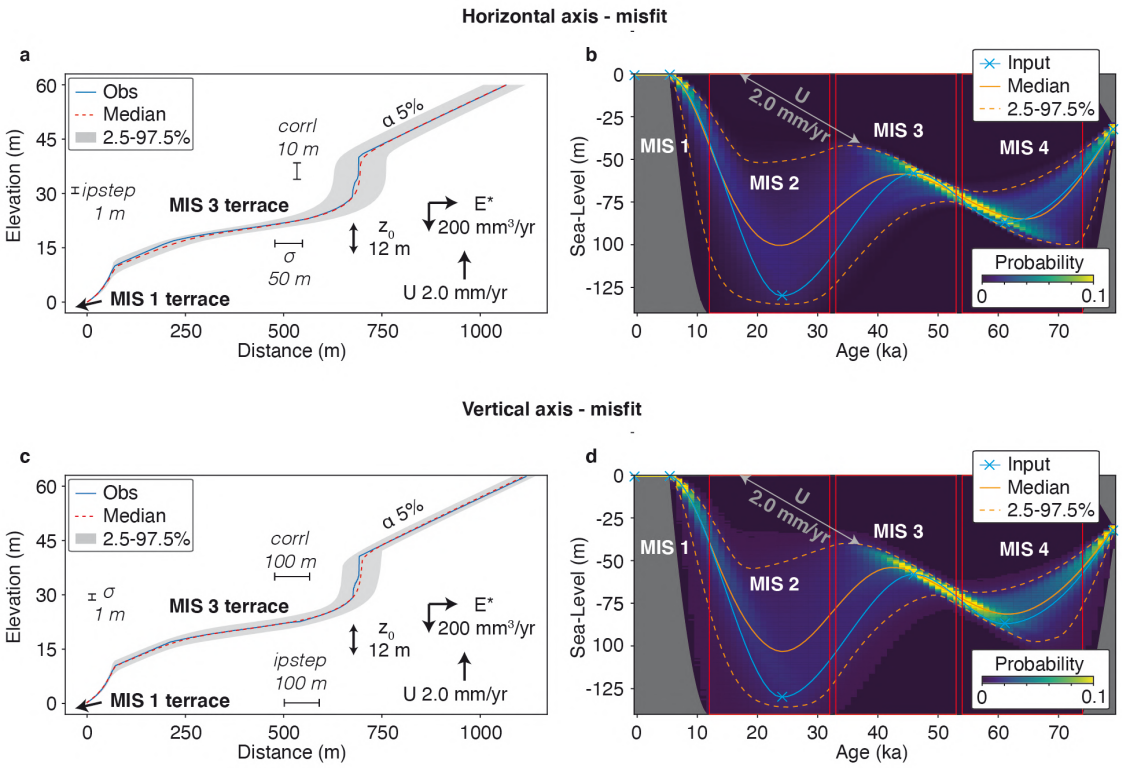

Figure S1 Comparison for misfit calculation on the horizontal (above; same as Fig. 2a,b) and vertical axis (below). Note that the paleo sea-level reconstruction is very similar, but the horizontal and vertical 95% distribution is slightly different.

Fig. 2a

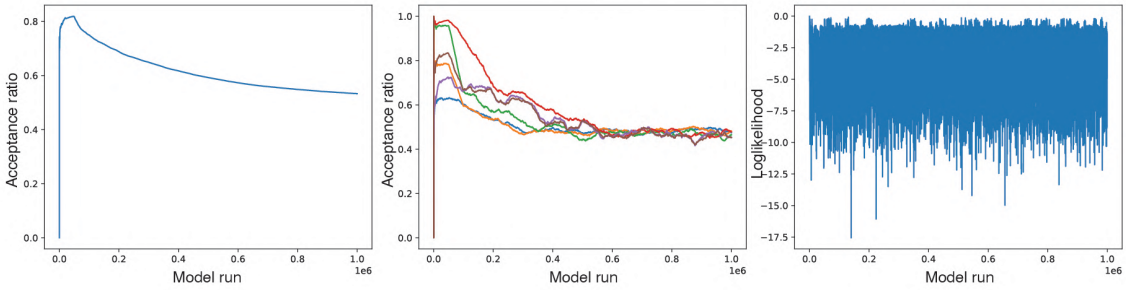

Fig. 2b

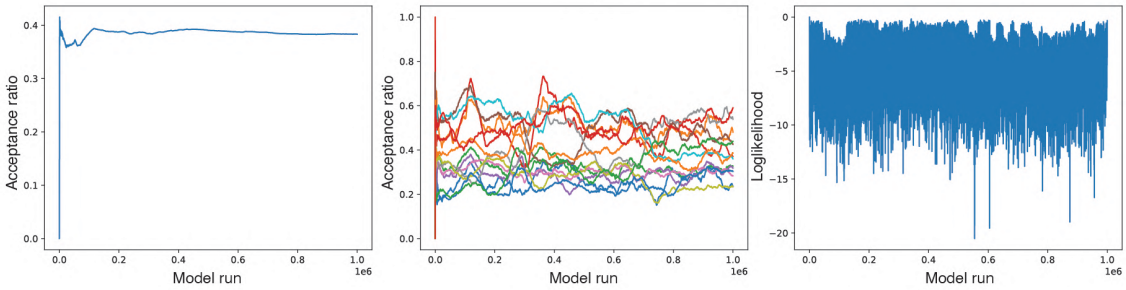

Fig. 2c

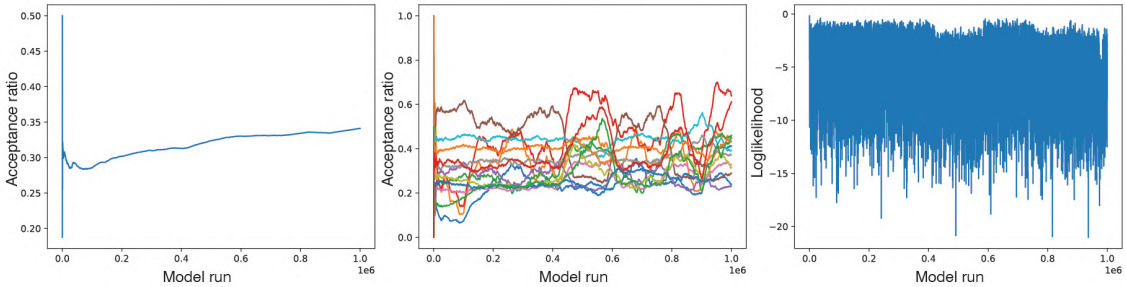

Fig. 2d

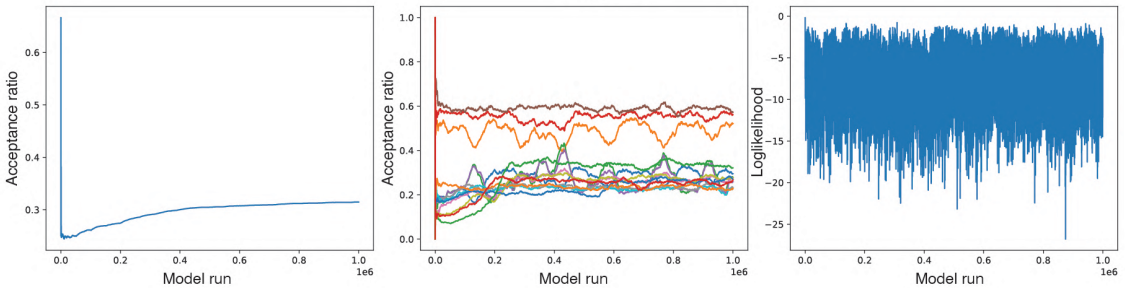

Fig. 3

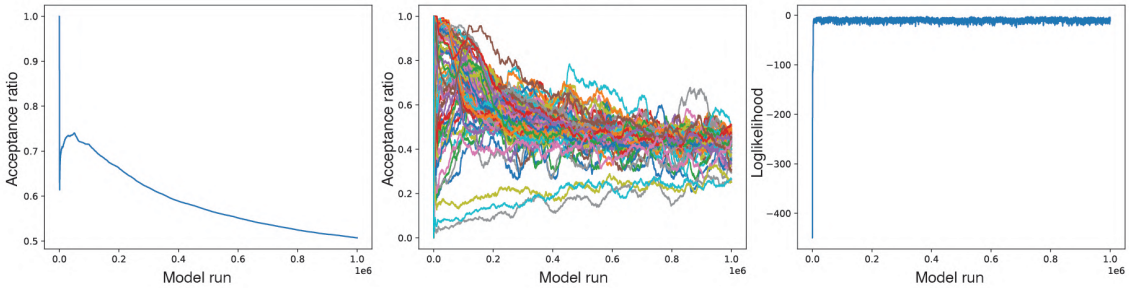

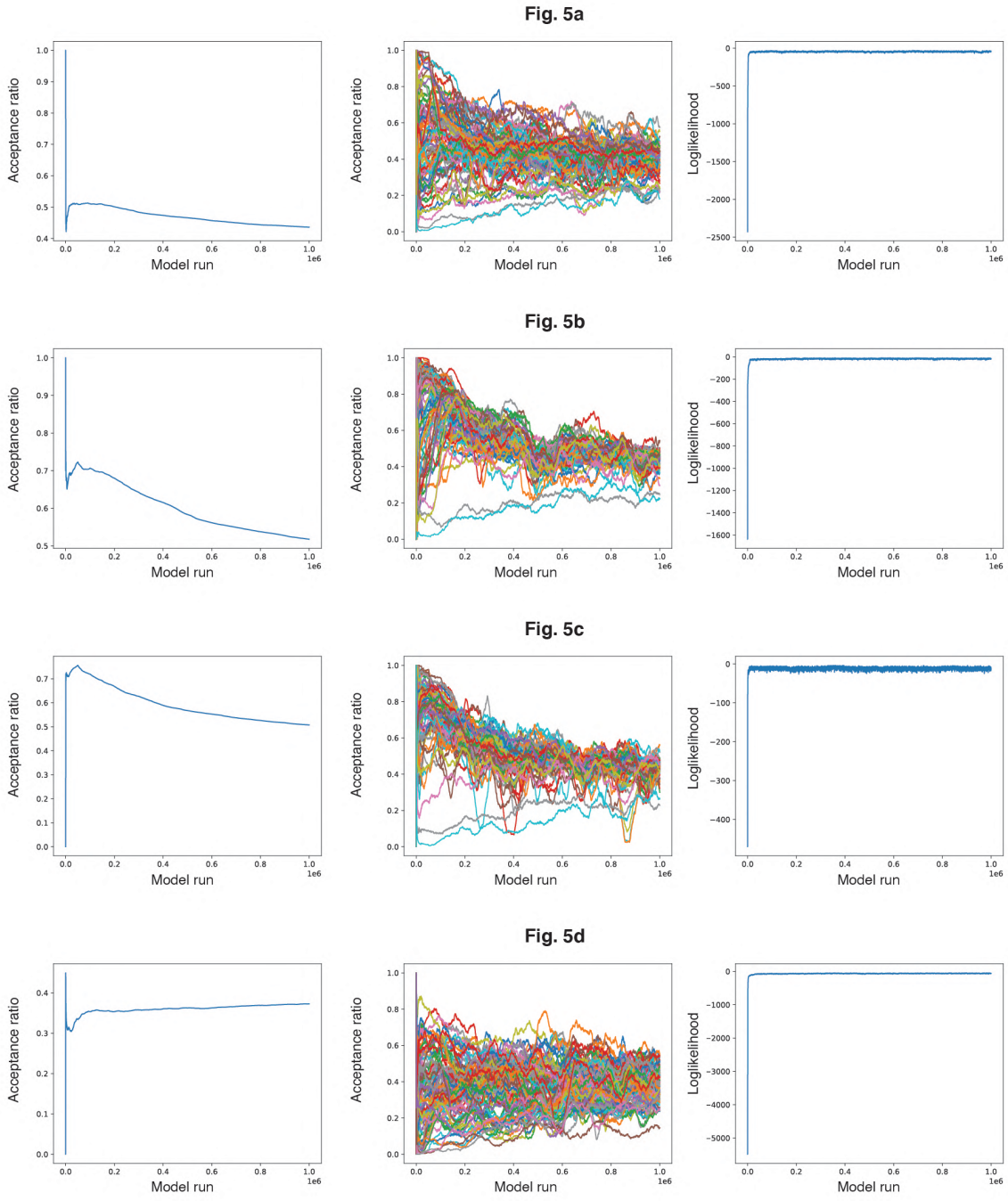

Figure S2. Average acceptance ratios for all inverted parameters (left), acceptance ratios for all individual inverted parameters (middle) and log-likelihood values (right) obtained during the 1 million model runs for the different models presented in the main paper Figures 2a-d, 3 and 5a-d.

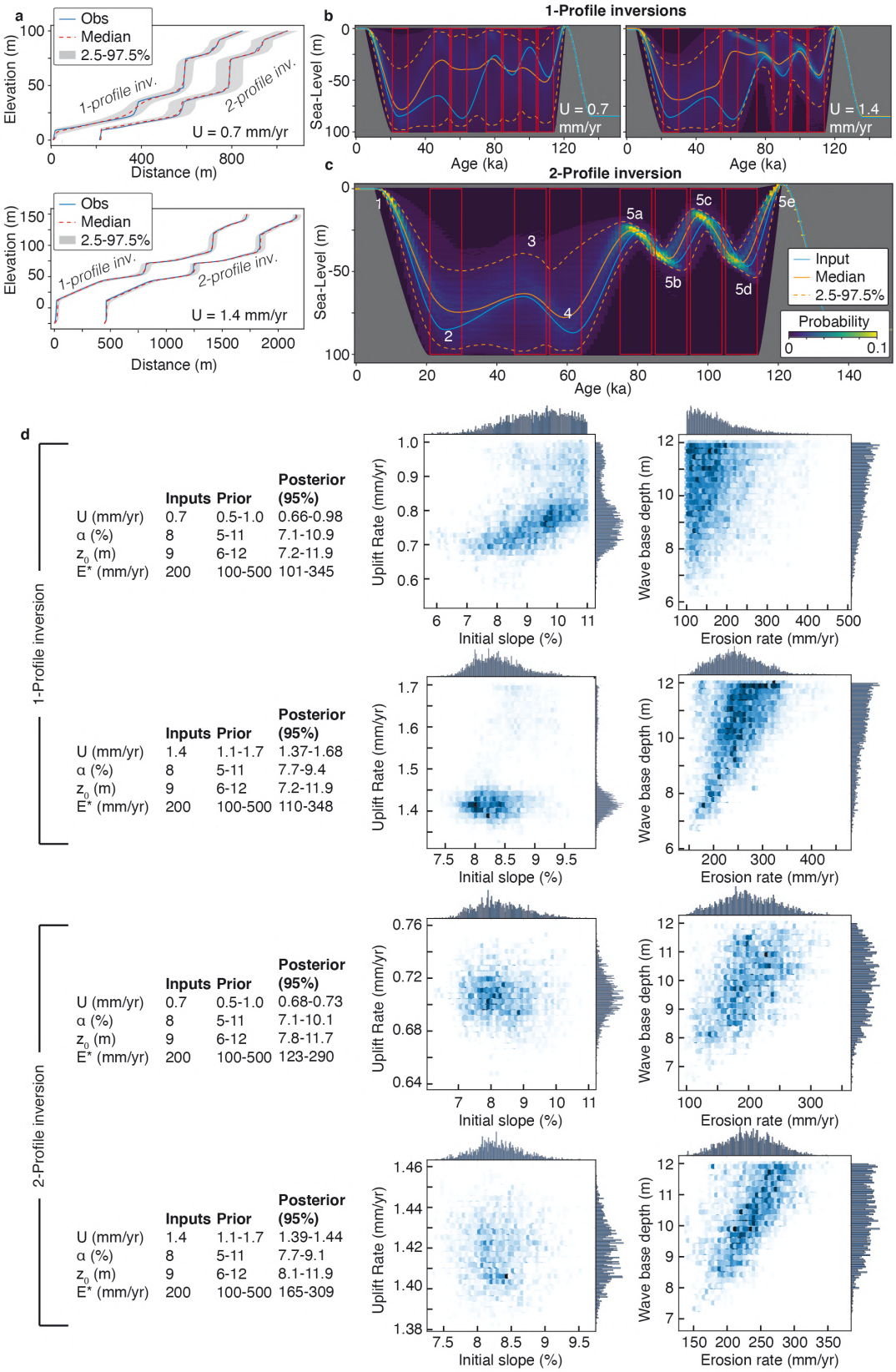
a
Obs
Median
2.5-97.5%
1-profile inv.
2-profile inv.
U = 0.7 mm/yr
Elevation (m)
Distance (m)
U = 1.4 mm/yr
b
1-Profile inversions
Sea-Level (m)
Age (ka)
U = 0.7 mm/yr
U = 1.4 mm/yr
c
2-Profile inversion
1
2
3
4
5a
5b
5c
5d
5e
Input
Median
2.5-97.5%
Probability
d
1-Profile inversion
Inputs Prior Posterior (95%)
U (mm/yr) 0.7 0.5-1.0 0.66-0.98
α (%) 8 5-11 7.1-10.9
z0 (m) 9 6-12 7.2-11.9
E* (mm/yr) 200 100-500 101-345
Inputs Prior Posterior (95%)
U (mm/yr) 1.4 1.1-1.7 1.37-1.68
α (%) 8 5-11 7.7-9.4
z0 (m) 9 6-12 7.2-11.9
E* (mm/yr) 200 100-500 110-348
2-Profile inversion
Inputs Prior Posterior (95%)
U (mm/yr) 0.7 0.5-1.0 0.68-0.73
α (%) 8 5-11 7.1-10.1
z0 (m) 9 6-12 7.8-11.7
E* (mm/yr) 200 100-500 123-290
Inputs Prior Posterior (95%)
U (mm/yr) 1.4 1.1-1.7 1.39-1.44
α (%) 8 5-11 7.7-9.1
z0 (m) 9 6-12 8.1-11.9
E* (mm/yr) 200 100-500 165-309
Uplift Rate (mm/yr)
Initial slope (%)
Wave base depth (m)
Erosion rate (mm/yr)

Figure S3 (Previous page). Tests with synthetic profiles similar to those in Fig. 2b-d, but with larger prior ranges for Uplift Rate (UR), Initial Slope (IS), Wave Base Depth (z_0) and Erosion Rate (E). Note that posterior ranges are consistently smaller for the 2-profile inversion than for the individual profile inversions.

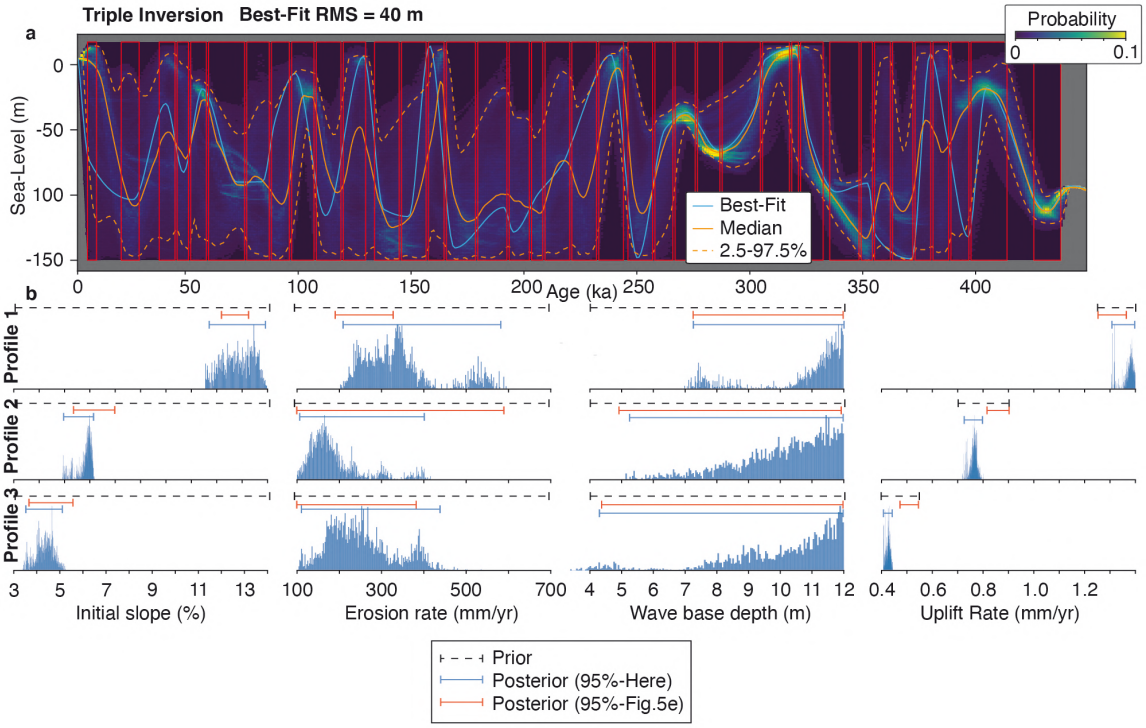

Figure S4. a) Triple inversion of the Corinth terraces, similar to the one presented in Fig. 5, but with all sea-/lake-level priors with a range of -150 to +15 m elevation to provide more freedom. Although misfit slightly increases (from 46 m to 40 m), posterior ranges are very broad, and reveal very little about the evolution of sea- and lake-levels in the Gulf/Lake Corinth. **b)** posterior ranges of other parameters. These ranges remain similar to those of Fig. 5.

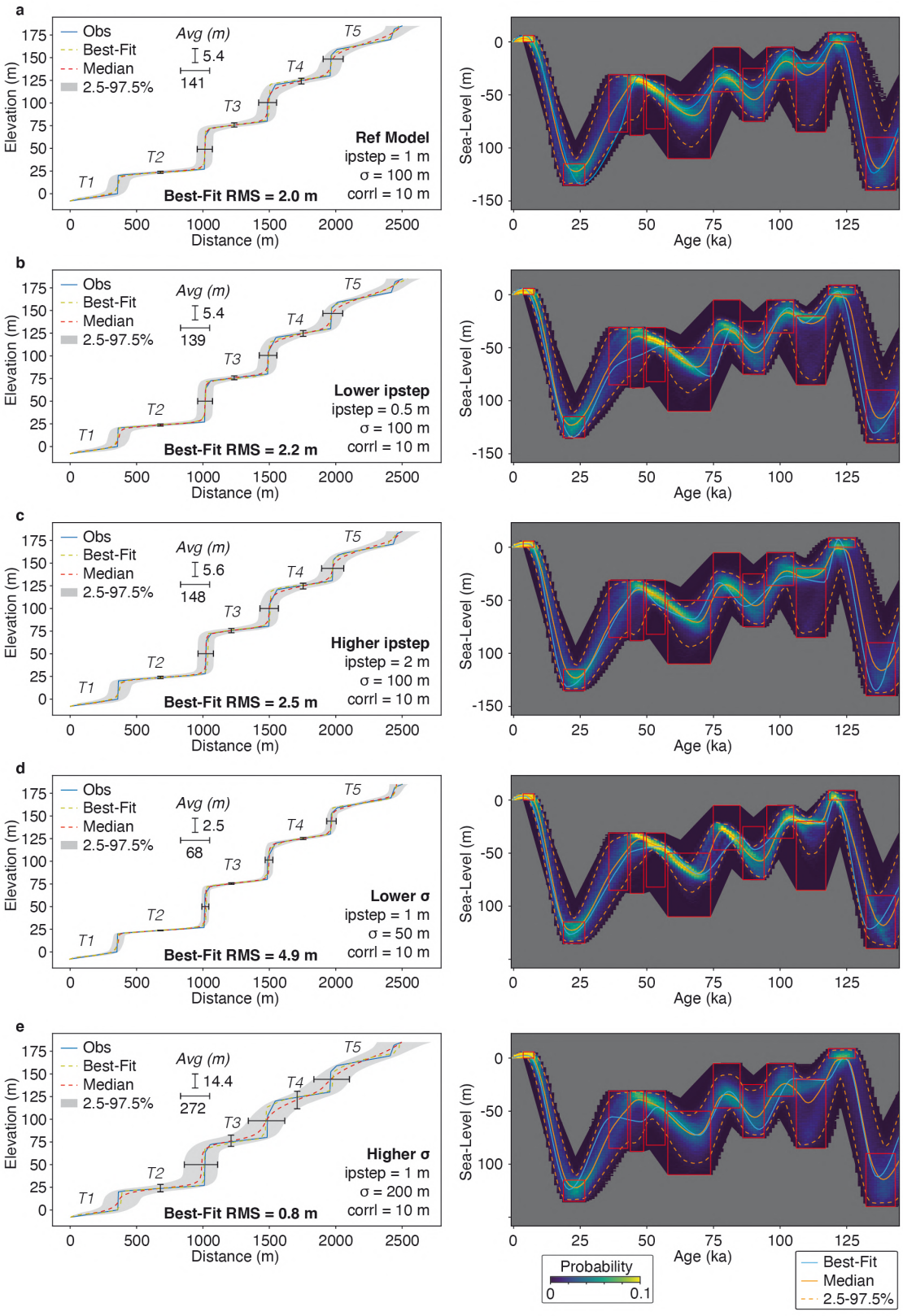
a
Obs
Best-Fit
Median
2.5-97.5%
Avg (m)
5.4
141
T1
T2
T3
T4
T5
Ref Model
ipstep = 1 m
σ = 100 m
corrl = 10 m
Best-Fit RMS = 2.0 m
Elevation (m)
Distance (m)
Sea-Level (m)
Age (ka)
b
5.4
139
Lower ipstep
ipstep = 0.5 m
σ = 100 m
corrl = 10 m
Best-Fit RMS = 2.2 m
c
5.6
148
Higher ipstep
ipstep = 2 m
σ = 100 m
corrl = 10 m
Best-Fit RMS = 2.5 m
d
2.5
68
Lower σ
ipstep = 1 m
σ = 50 m
corrl = 10 m
Best-Fit RMS = 4.9 m
e
14.4
272
Higher σ
ipstep = 1 m
σ = 200 m
corrl = 10 m
Best-Fit RMS = 0.8 m
Probability
0
0.1
Best-Fit
Median
2.5-97.5%

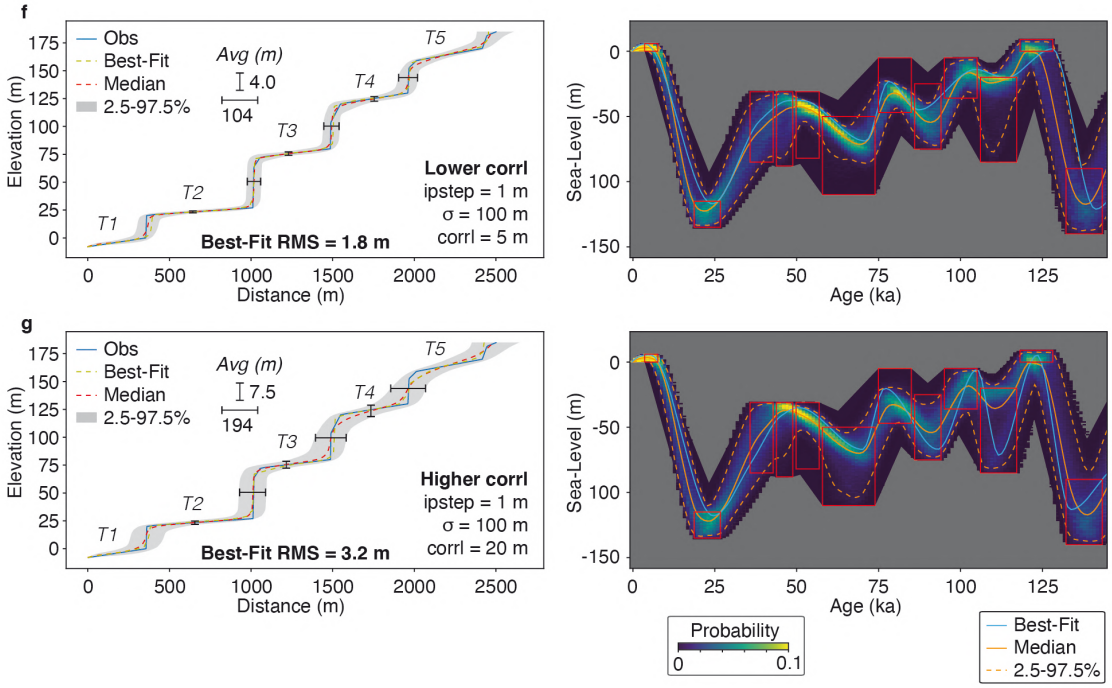

Figure S5. Santa Cruz terrace sequence tests with different inversion parameters. **a)** Same as Fig. 3, for comparison with inversions that use a **b)** lower ipstep, **c)** higher ipstep, **d)** lower σ, **e)** higher σ, **f)** lower corrl and **g)** higher corrl. Note that the ranges for accepted terrace profiles, in terms of average horizontal and vertical 95% posterior distribution, tend to increase or decrease (left side), but the range of sea-level does not change much (right side).

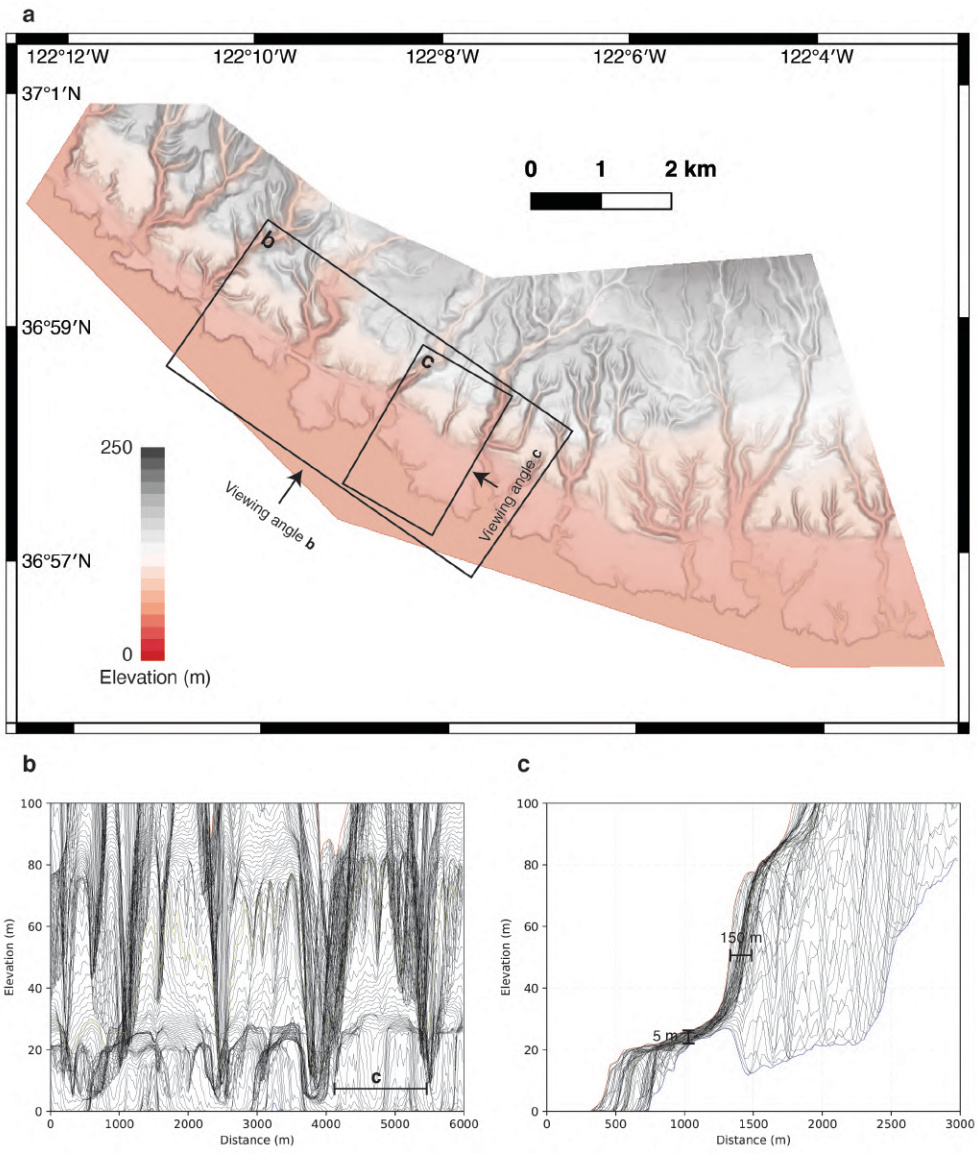

Figure S6. Santa Cruz marine terrace sequence morphology. **a)** Map of the marine terrace sequence NW of the town of Santa Cruz (California, US), based on a Digital Elevation Model provided in Jara-Muñoz et al. (2019), plotted in QGIS3. **b)** 300 Stacked swath profiles of the area shown in **a**, as viewed from the SW, showing the lateral variability in terrace elevations, and **c)** 150 stacked swath profiles of the area shown in **a** and **b**, as viewed from the SE, showing the variability in terrace elevation and terrace width within the specific cross-section (compare with Fig. S3).

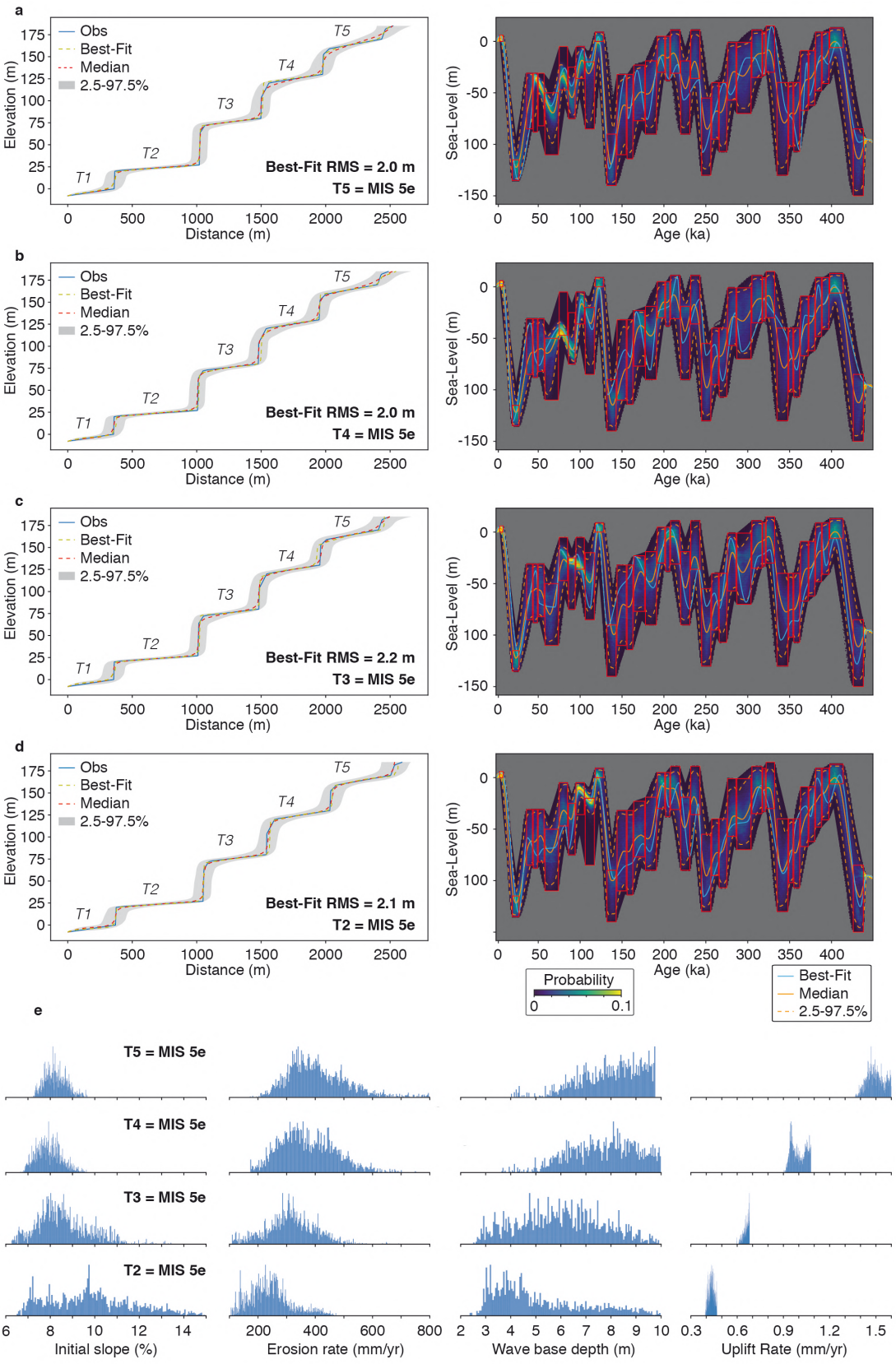
a
Obs
Best-Fit
Median
2.5-97.5%
T1
T2
T3
T4
T5
Best-Fit RMS = 2.0 m
T5 = MIS 5e
Elevation (m)
Distance (m)
Sea-Level (m)
Age (ka)
b
Best-Fit RMS = 2.0 m
T4 = MIS 5e
c
Best-Fit RMS = 2.2 m
T3 = MIS 5e
d
Best-Fit RMS = 2.1 m
T2 = MIS 5e
Probability
0
0.1
e
T5 = MIS 5e
T4 = MIS 5e
T3 = MIS 5e
T2 = MIS 5e
Initial slope (%)
Erosion rate (mm/yr)
Wave base depth (m)
Uplift Rate (mm/yr)

Figure S7 (Previous page). Santa Cruz terrace sequence tests with different uplift rates. **a)** Same as Fig. 3, for comparison with inversions that use an uplift rate of **b)** 0.9-1.1 mm/yr, **c)** 0.5-0.7 mm/yr, and **d)** 0.3-0.5 mm/yr **e)** Ranges of initial slope, erosion rate, wave base depth and uplift rate that correspond to the four scenarios in **a-d**

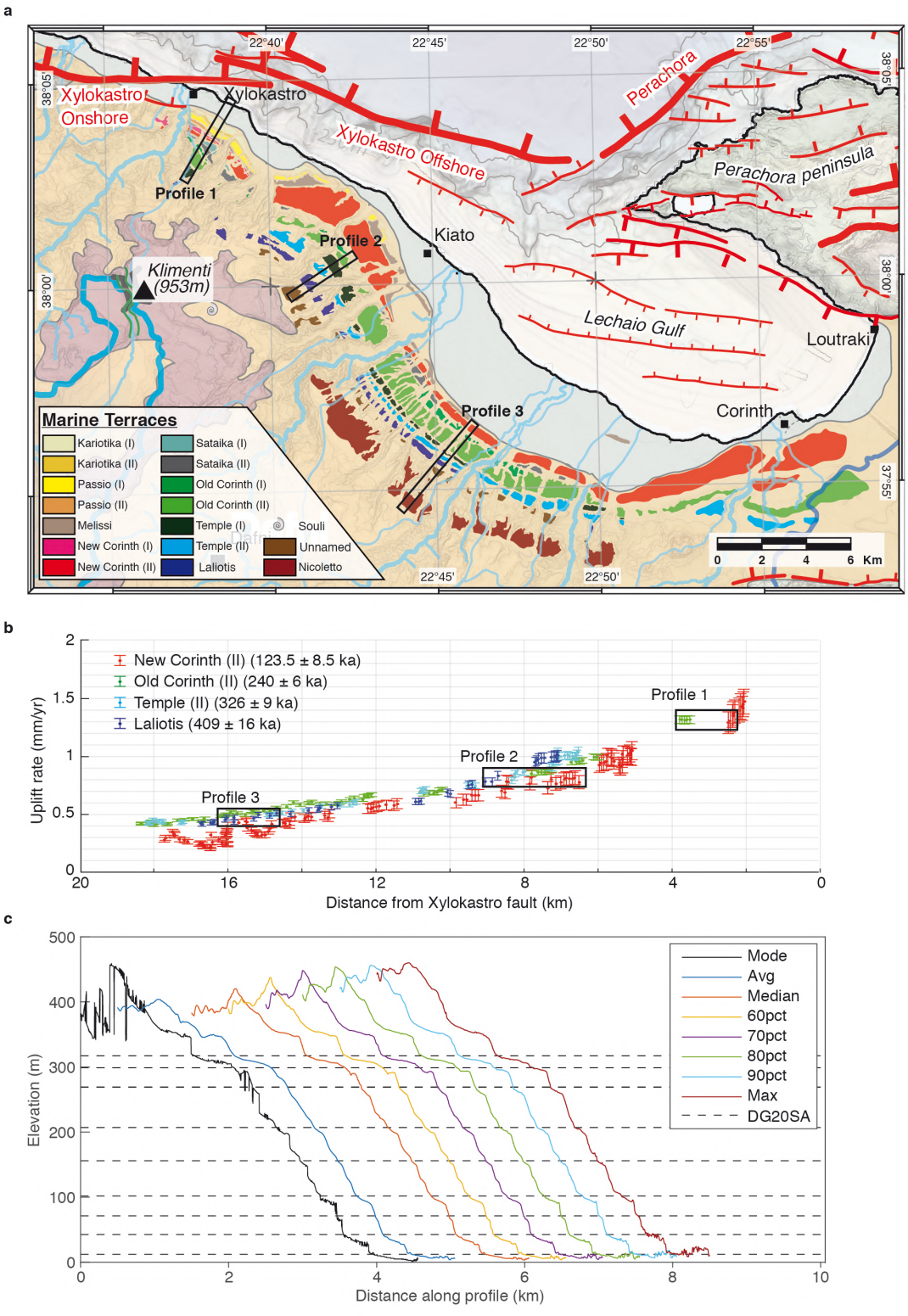
a
22°40'
22°45'
22°50'
22°55'
38°05'
38°00'
37°55'
Xylokastro Onshore
Xylokastro
Xylokastro Offshore
Perachora
Perachora peninsula
Profile 1
Profile 2
Profile 3
Kiato
Klimenti (953m)
Lechaio Gulf
Loutraki
Corinth
Marine Terraces
Kariotika (I)
Kariotika (II)
Passio (I)
Passio (II)
Melissi
New Corinth (I)
New Corinth (II)
Sataika (I)
Sataika (II)
Old Corinth (I)
Old Corinth (II)
Temple (I)
Temple (II)
Laliotis
Souli
Unnamed
Nicoletto
0 2 4 6 Km
b
New Corinth (II) (123.5 ± 8.5 ka)
Old Corinth (II) (240 ± 6 ka)
Temple (II) (326 ± 9 ka)
Laliotis (409 ± 16 ka)
Profile 1
Profile 2
Profile 3
Uplift rate (mm/yr)
Distance from Xylokastro fault (km)
c
Mode
Avg
Median
60pct
70pct
80pct
90pct
Max
DG20SA
Elevation (m)
Distance along profile (km)

Figure S8 (Previous page). SE Corinth Rift terraces. **a)** Map of the SE Corinth Rift (modified from De Gelder et al., 2019) with locations of the inverted profiles. **b)** Uplift rates as a function of distance from the fault (modified from De Gelder et al., 2019) with locations of the inverted profiles. **c)** Different characterizations of the topography within the profiles of a, compared to the average shoreline angle elevations calculated in De Gelder et al. (2020).